coatings

MDPI

Article

Non-Precious Metals Catalysts for Hydrogen Generation

Zita Sukackienė *, Gitana Valeckytė, Virginija Kepenienė, Irena Stalnionienė, Vitalija Jasulaitienė, Jūratė Vaičiūnienė, Loreta Tamašauskaitė-Tamašiūnaitė *, Giedrius Stalnionis and Eugenijus Norkus

Department of Catalysis, Center for Physical Sciences and Technology (FTMC), Saulėtekio av. 3, LT-10257 Vilnius, Lithuania; gitana.valeckyte@ftmc.lt (G.V.); virginija.kepeniene@ftmc.lt (V.K.); irena.stalnioniene@ftmc.lt (I.S.); vitalija.jasulaitiene@ftmc.lt (V.J.); jurate.vaiciuniene@ftmc.lt (J.V.); giedrius.stalnionis@ftmc.lt (G.S.); eugenijus.norkus@ftmc.lt (E.N.)

* Correspondence: zita.sukackiene@ftmc.lt (Z.S.); loreta.tamasauskaite@ftmc.lt (L.T.-T.)

Abstract: In this paper, the generation of hydrogen from alkaline sodium borohydride solution by hydrolysis is studied. To obtain catalysts for efficient hydrogen generation, Ni, Mn, Mo, and Co metals were deposited on the Cu surface by the simple electroless metal deposition method using morpholine borane as a reducing agent. Depending on the peculiarities of the deposition of each metal, the coating thickness was ca. 1 μm for all catalysts. The deposited coatings were compact and crack-free, with multilayer characteristics and a cauliflower-like structure. The prepared Ni/Cu, NiMn/Cu, NiMo/Cu, NiCo/Cu, NiCoMn/Cu, NiCoMo/Cu, and NiCoMoMn/Cu catalysts showed an efficient catalytic activity for sodium borohydride hydrolysis reaction. The lowest activation energy of 45.3 kJ mol^{-1} for sodium borohydride hydrolysis reaction was obtained using the NiCoMoMn/Cu catalyst. The highest hydrogen generation rate of 3.08 mL min^{-1} was also achieved using this catalyst at 303 K. With a further increase in temperature to 343 K, the hydrogen generation rate catalyzed by the NiCoMoMn/Cu increased 7.7 times and reached 23.57 mL min^{-1}.

Keywords: electroless deposition; nickel; cobalt; molybdenum; manganese; hydrogen generation; borohydride

check for updates

Citation: Sukackienė, Z.; Valeckytė, G.; Kepenienė, V.; Stalnionienė, I.; Jasulaitienė, V.; Vaičiūnienė, J.; Tamašauskaitė-Tamašiūnaitė, L.; Stalnionis, G.; Norkus, E. Non-Precious Metals Catalysts for Hydrogen Generation. *Coatings* **2023**, *13*, 1740. https://doi.org/10.3390/coatings13101740

Academic Editor: Ioannis V. Yentekakis

Received: 29 August 2023
Revised: 25 September 2023
Accepted: 5 October 2023
Published: 7 October 2023

Copyright: © 2023 by the authors. Licensee MDPI, Basel, Switzerland. This article is an open access article distributed under the terms and conditions of the Creative Commons Attribution (CC BY) license (https://creativecommons.org/licenses/by/4.0/).

1. Introduction

For several decades, ways to replace fossil fuels such as oil, coal, and natural gas have been sought. The reason for finding alternatives to these materials is that they are constantly depleting, and burning products of such fuel pollutes the environment and causes the greenhouse effect, thus contributing to climate change. Therefore, new types of fuel and renewable energy sources have become increasingly studied by scientists. Hydrogen as an alternative to fossil fuels has been proposed for a long time, as hydrogen fuel cells already operate in the aviation, electrical, and automotive industries [1–7]. A few years ago, hydrogen demand was 94 million tons and accounted for about 2.5% of global final energy consumption. It is estimated that by 2030, hydrogen demand will increase by more than 1.5 times to reach more than 150 million tons, with nearly 30% of that demand coming from new applications [8]. However, the vast majority of current hydrogen (about 95%) is produced by steam methane reforming and coal gasification processes, which produce CO_2 and require carbon capture and storage to reduce the environmental impact [9,10]. In addition, fossil fuels are inevitably consumed. At the same time, due to the flammability and explosiveness of hydrogen, transportation and storage problems are encountered [1,4,7,11–13]. Therefore, great attention was focused on storing hydrogen in other materials and further generating it from them. One of the most important properties of hydrogen storage materials is their high gravimetric hydrogen capacity. Some of those materials could be liquid ammonia, various organic compounds, or solid materials such as metal hydrides, complex hydrides, organic hydrides, carbon-containing materials, zeolites, and metal-organic frameworks [3,5,13–15]. Due to their high hydrogen capacity

(for example, NH_3BH_3 (19.6 wt%), $LiBH_4$ (18.4 wt%), NH_3 (17.7 wt%), $N_2H_4BH_3$ (15.4 wt%), $Mg(BH_4)_2$ (14.8 wt%), $NaBH_4$ (10.73 wt%), and $N_2H_4 \cdot H_2O$ (8 wt%)), these materials are considered promising for hydrogen storage and use in portable fuel cells [5,14–16].

Sodium borohydride is considered one of the most suitable materials for hydrogen storage. It is characterized by a high hydrogen content, it is cheap, environment-friendly, stable in alkaline solutions, non-flammable, non-toxic, and works under mild conditions [6,7,11,12,15–19]. The generation of hydrogen from this hydride is described by the following reaction [6,7,20]:

$$NaBH_4 + 2H_2O \rightarrow 4H_2 + NaBO_2 + Q \quad (1)$$

Notably, the borohydride hydrolysis reaction produces extremely pure hydrogen, which can be directly used in the hydrogen fuel cell. Fuel cells using pure hydrogen have virtually no emissions other than water. Therefore, the discovery of selective catalysts for this reaction is an important part of the research to avoid the pollution of the electrode surface during the process and the disadvantages of storing and transporting hydrogen. Moreover, the less corrosive nature of an alkaline environment ensures potentially greater durability as well as inherently faster kinetics of the oxygen reduction reaction in an alkaline fuel cell (AFC), and allows the use of non-noble and low-cost metal electrocatalysts such as nickel, cobalt, molybdenum, etc., to make AFC a potentially low-cost technology compared to other fuel cells that use platinum catalysts [21]. Therefore, studies of the performance characteristics of alkaline fuel cells powered by hydrogen are important and relevant.

One of the most important reasons for the efficient operation of the energy source is a functional, effective, and relatively inexpensive catalytic material that initiates the onset of a chemical reaction. It is known that sodium borohydride hydrolyzes even at room temperature without a catalyst, but this reaction is very slow [6,12,15,17–20]. Noble metals, such as Pt, Ru, Pd, Rh, and Au were found to be great and efficient catalysts to accelerate sodium borohydride hydrolysis [7,11,12,17–19,22]. However, due to their high price, low abundance, and rapid surface poisoning, there appears to be a need to create new catalysts and replace noble metals. Therefore, much effort has been devoted to developing new, efficient catalytic materials and improving their functionalization while addressing the use of expensive noble metals and ecological problems to create cleaner fuel technologies and eliminate environmentally harmful processes in the chemical industry. The search strategy for new catalysts is based on developing alternative, more effective materials using transition metals including Ni, Co, Fe, Mn, Cu, and Mo [17–19,23–25]. The literature indicates that joining metals together improves the catalytic properties of the new catalyst due to the synergistic effect between metals or changes in the surface structure with the participation of several metals, thereby creating the possibility of obtaining effective catalysts that can replace precious metals [26–28]. It is also reported that even a small amount of manganese in coatings improves its catalytic properties. It is believed that the presence of Mn results in the formation of nanosphere structures with larger exposed surfaces, leading to an improvement in the catalytic performance of the catalyst, which may also be related to the altered electrical structure of the catalyst [29]. Some different methods can be used to obtain pure metal films or coatings. Z. Liang at al. proposed Ni deposited on the ferrite powder using the impregnation–chemical reduction method [30]. M.S. Akkus presented Ni, NiCr, and NiV catalysts prepared by the magnetron sputtering process [27]. J.C. Ingerloll at al. deposited the NiCo as powder using a chemical reduction method by using $NaBH_4$ and metal chlorides [31]. They reported that this catalyst exhibited 62 kJ mol^{-1} activation energy of the borohydride hydrolysis reaction [31].

Electroless metal plating systems are based on the autocatalytic reduction of metals using a reducing agent [32–35]. It is generally agreed that the reducing agent is adsorbed on the metal surface because the metal (Cu) catalyzes the anodic oxidation of the reducing agent. During this reaction, the generated electrons reduce the metal ions or metal ion complexes adsorbed on the surface. Mostly, the reaction itself is autocatalytic, i.e., the new metal coating formed catalyzes the oxidation of the reducing agent and the metal deposition continues. The metal plating solution typically consists of metal ions, a reducing

agent, appropriate complexing agents, and stabilizers. The most important research was carried out in 1946 by A. Brenner and G. E. Riddell, who obtained a NiP coating by electroless nickel plating using sodium hypophosphite as a reducing agent [34–37]. Sodium hypophosphite and morpholine borane are the most commonly used reducing agents used in electroless nickel plating baths [37,38]. However, boron-containing compounds are stronger reducing agents compared to hypophosphites because they give six or eight electrons to the reduction of metals. There are some reducing agents containing boron available for electroless deposition of non-precious metals. Sodium borohydride is the most popular reducing agent; however, the main disadvantage of electroless plating solutions with $NaBH_4$ as a reducing agent is that a high deposition rate is obtained only at elevated temperatures (90–95 °C) and in strong alkaline media (pH 12–14). The application of boron-nitrogen compounds—borazanes, e.g., dimethylamineborane, as reducing agents allows the deposition process to be carried out in a wide pH and temperature range. However, recently, morpholine borane (MB, $C_4H_8ONH{\cdot}BH_3$) was proposed as a reducing agent for electroless metal deposition and a source for boron due to its lower volatility and toxicity compared to dimethylamineborane [39].

This electroless metal deposition method has proven successful due to its low initial investment, simple coating conditions, and good results. This method produced a uniform metallic coating with excellent properties on substrates of various shapes and sizes, such as Ni foam, stainless steel mesh, aluminum oxide membranes, carbon materials, Cu sheets, and foam [32,34,36,37,40–48].

Electroless metal deposition covers many metals: Ni, Co, Cu, Pt, Pd, Ru, Rd, W, Ir, Zn, Ba, Mo, Au, and Ag [34,35,41–43]. However, combining several metals in the same coating, especially non-noble metals, with an efficient activity for the reaction required remains a challenge for scientists. There are currently four described Ni coatings combined with other metals: NiCu, NiCo, NiFe, and NiCoMo, investigated for hydrogen generation from sodium borohydride. However, the reported activation energy values are quite high [43–46,49]. J.C. Ingerloll et al. report that the NiCo catalyst exhibits 62 kJ mol^{-1} activation energy for the borohydride hydrolysis reaction [31]. L. Wang et al. present the four-component CoNiMoP/g-Al_2O_3 catalyst with 52 kJ mol^{-1} activation energy for the borohydride hydrolysis reaction.

In this work, we present different composition coatings where Ni, Co, Mn, and Mo were deposited on the Cu sheet surface by electroless metal deposition. The composition of bi- (NiCo, NiMn, and NiMo), ternary- (NiCoMn, NiCoMo), and four-component (NiCoMnMo) coatings was characterized using inductively coupled plasma optical emission spectroscopy (ICP-OES), field-emission scanning electron microscopy (FESEM), and X-ray photoelectron spectroscopy (XPS). The catalytic activity of prepared NiMn/Cu, NiMo/Cu, NiCo/Cu, NiCoMn/Cu, NiCoMo/Cu, and NiCoMoMn/Cu catalysts was investigated for hydrogen generation reaction from alkaline sodium borohydride solution via hydrolysis at different temperatures. For comparison, a pure Ni/Cu catalyst was also prepared under the same conditions for the same investigation.

2. Materials and Methods

2.1. Chemicals

Copper foil (Cu, 99.8% purity), sodium molybdate dihydrate ($Na_2MoO_4{\cdot}2H_2O$, 99.5%), and manganese acetate $(CH_3COO)_2Mn$, 99%) were purchased from Sigma-Aldrich, Louis, MO, USA. Sulfuric acid (H_2SO_4, 96%), hydrochloric acid (HCl, 35%–38%), nickel sulfate hexahydrate ($NiSO_4{\cdot}6H_2O$, 98%), cobalt sulfate heptahydrate($CoSO_4{\cdot}7H_2O$, 99.5%), morpholine borane ($C_4H_8ONH{\cdot}BH_3$, 97%), glycine (NH_2CH_2COOH, 99.5%), sodium citrate CH_3COONa, and KOH (98.8%) were purchased from Chempur Company (Karlsruhe, Germany). All chemicals were of analytical grade and used directly without further purification.

2.2. Fabrication of Catalysts

The electroless deposition of Ni, NiMn, NiMo, NiCo, NiCoMn, NiCoMo, and NiCoMoMn coatings is based on the investigated Ni deposition bath [50,51]. This was performed on the Cu sheet (1 cm × 1cm), using morpholine borane (MB) as a reducing agent as described [50,51]. The electroless plating solution composition and the deposition parameters of coatings are given in Table 1. Before the electroless plating, the surface of Cu sheets were pre-treated with 50%–100% calcium magnesium oxide, known as "Vienna Lime" (Kremer Pigments GmbH & Co. KG, Aichstetten, Germany), rinsed with deionized water and held in 10% HCl solution for 1 min to remove inorganic impurities and washed again. Cleaned Cu sheets were activated with Pd(II) ions by immersing them in a 0.5 g L^{-1} $PdCl_2$ solution for 5 s, then rinsed again with deionized water and placed into an electroless plating solution. The coatings were deposited from a freshly prepared solution (Table 1) at temperatures from 40 °C to 60 °C. In all cases, the pH of the plating solutions was 7 (measured at room temperature). The deposition time varied from 5 to 50 min to obtain the same coating thickness. The gravimetrically determined thickness of deposited coatings was 1 µm for all investigated coatings.

Table 1. Composition of electroless plating solution and deposition parameters of catalysts.

Catalysts	Plating Solution Composition (mol L^{-1}) and Plating Conditions									
	$NiSO_4$	CH_3COONa	MB	Glycine	$(CH_3COO)_2Mn$	Na_2MoO_4	$CoSO_4$	pH	T, °C	t, min
Ni/Cu	0.05	0.04	0.05	0.4	-	-	-		40	50
NiMn/Cu	0.1	0.04	0.2	-	0.07	-	-		40	30
NiMo/Cu	0.1	0.04	0.2	-	-	0.001	-		50	12
NiCo/Cu	0.1	-	0.2	0.3	-	-	0.1	7	50	5
NiCoMn/Cu	0.1	0.04	0.2	-	0.07	-	0.1		60	10
NiCoMo/Cu	0.1	0.04	0.2	-	0.07	0.001	0.1		50	10
NiCoMoMn/Cu	0.1	0.04	0.2	-	0.07	0.001	0.1		60	6

2.3. Characterization of Catalysts

The surface morphology of the samples was characterized using SEM/FIB Workstation Helios Nanolab 650 (FEI, Hillsboro, OR, USA) arranged with an energy-dispersive X-ray (EDX) spectrometer INCA Energy 350X-Max 20 (Oxford Instruments, Halifax, UK). An ICP-OES analysis was conducted using an inductively coupled plasma optical emission spectrometer Optima 7000DV (PerkinElmer, Shelton, CT, USA) to confirm the content of all metals in the coatings.

The surface elemental composition of the obtained Ni, NiMn, NiMo, NiCo, NiCoMn, NiCoMo, and NiCoMoMn coatings was determined by employing X-ray photoelectron spectroscopy (XPS) using an "ESCALABMKII" spectrometer (VG Scientific, East Grinstead, UK) equipped with an Al Kα X-ray radiation source (1486.6 eV) operated at a fixed pass energy of 20 eV.

2.4. Measurements of Hydrolysis of $NaBH_4$

The volume of the generated hydrogen (H_2) catalyzed by the prepared catalysts was measured using a MilliGascounter (Type MGC-1 V3.2 PMMA, Ritter, Bochum, Germany) connected to a personal computer. A thermostated airtight flask fitted with an outlet connected to the MilliGascounter was used to collect the generated H_2 gas. The reaction bath contained 15 mL of 5 wt% $NaBH_4$ + 0.4 wt% NaOH solution. In all the measurements, the prepared catalysts were placed in an alkaline sodium borohydride solution of designated temperature and stirred with a magnetic stirrer. The hydrogen generation rate (HGR) was measured at a working solution in the 303 to 343 K temperature range to determine the activation energy. For the calculation of the activation energy of each catalyst, the Arrhenius equation graph (dependence of the reaction rate to the temperature) was used. Knowing the amount of hydrogen evolution after 60 min at each temperature, the rate of hydrogen gas released during the reaction (k) was calculated. Then the activation energy of the electrochemical process (E_A, kJ·mol^{-1}) was calculated using the given formula.

3. Results and Discussions

3.1. Microstructure and Morphology Studies

This work aimed to use a simple method to prepare effective catalysts for hydrogen generation from an alkaline sodium borohydride solution. For this purpose, Ni, NiMn, NiMo, NiCo, NiCoMn, NiCoMo, and NiCoMoMn were deposited on the Cu sheets using a simple electroless deposition method with morpholine borane as a reducing agent obtaining catalysts with a ca. 1 µm thickness coating. The morphology and particle size of the prepared catalysts were estimated by FESEM. Figure 1 represents FESEM images of catalysts of different compositions. It is clearly seen that all formed coatings are compact and crack-free with characteristic multilayer, cauliflower-like structures (Figure 1a–g). The FESEM images also reveal that all prepared coatings, Ni/Cu, NiMn/Cu, NiMo/Cu, NiCo/Cu, NiCoMn/Cu, NiCoMo/Cu, and NiCoMoMn/Cu (Figure 1a–g), consist of particles of different sizes, which coalesce into oval-shaped agglomerates. It can be seen that the Ni/Cu surface is the most smooth (Figure 1a). Adding additional metal causes the growth of agglomerates on the surface in an average size range of 40 nm to 1.6 µm.

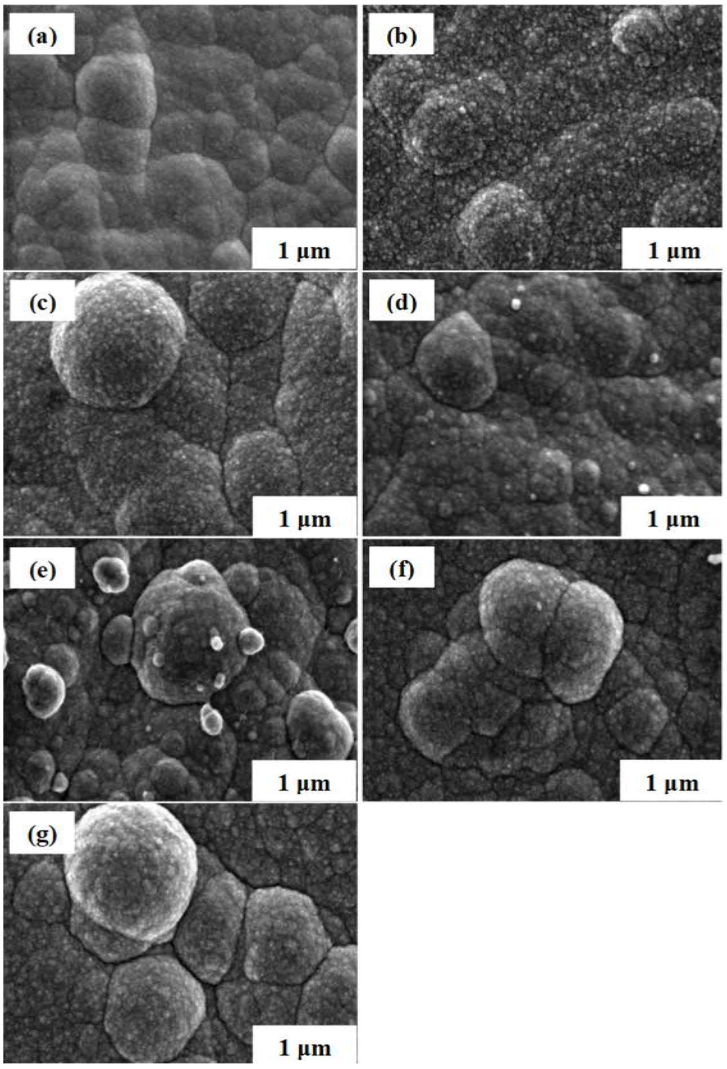

Figure 1. FESEM images of prepared Ni/Cu (**a**), NiMn/Cu (**b**), NiMo/Cu (**c**), NiCo/Cu (**d**), NiCoMn/Cu (**e**) NiCoMo/Cu (**f**), and NiCoMoMn/Cu (**g**) catalysts.

The amounts of metals in prepared catalysts calculated from ICP-OES data are presented in Table 2. As can be seen from the presented data, when Ni and Co are co-

precipitated, the cobalt deposition rate is much faster. About 10%–20% of Ni remains in the coatings compared with pure Ni/Cu. The quantity of Co in the prepared catalyst varies in the range of 77.39–90.18 wt%. Quantities of Mo ca. 14.54, 10.1, and 7.33 wt% were incorporated in the NiMo, NiCoMo, and NiCoMoMn coatings, respectively. In the case of NiMn/Cu, NiCoMn/Cu, and NiCoMoMn/Cu catalysts, the quantity of Mn was significantly small and equal to ca. 0.16, 0.01 and 0.01 wt%, respectively. It should be mentioned that it is difficult to deposit a larger quantity of manganese because the redox potential for Mn^{2+} to become Mn^0 ($Mn^{2+} + 2e^- \rightarrow Mn^0$) is very negative (−1.185 V); therefore, it is difficult to reduce Mn^{2+} into Mn^0 through a redox reaction.

Table 2. Element composition and metal loading of the prepared coatings deposited on Cu surface analyzed by ICP-OES.

Catalysts	Element, wt%				Element Loadings, μg cm^{-2}			
	Ni	Mn	Mo	Co	Ni	Mn	Mo	Co
Ni/Cu	100	-	-	-	373.7	-	-	-
NiCo/Cu	22.61	-	-	77.39	179.35	-	-	614
NiMn/Cu	99.84	0.16	-	-	475.15	0.745	-	-
NiMo/Cu	85.46	-	14.54	-	419.05	-	71.3	-
NiCoMn/Cu	9.81	0.01	-	90.18	59.75	0.06	-	549.5
NiCoMo/Cu	8.01	-	10.1	81.89	37.18	-	46.875	380.1
NiCoMoMn/Cu	7.95	0.01	7.33	84.71	32.515	0.05	29.985	346.65

3.2. XPS Analysis of Prepared Catalysts

The elemental composition of the prepared Ni/Cu, NiCo/Cu, NiMn/Cu, NiMo/Cu, NiCoMn/Cu, NiCoMo/Cu, and NiCoMoMn/Cu catalysts was determined by XPS. Figures 2 and 3 present the high-resolution Ni2p, Co2p, Mo3d, and O1s spectra of each coating. It has to be mentioned that the Mn2p spectra were not detected by XPS analysis due to a very low amount (according to ICP-OES) of Mn in the coatings. The XPS analysis was also carried out in a 40-μm-deep etching.

In general, typical XPS spectra with spin-orbital splitting transition peaks indicative of pure metals were observed for all investigated catalysts (Figures 2 and 3). The most expressed Ni $2p_{3/2}$ binding energy peak originated at 852.7–852.9 eV and corresponds to Ni^0 (Figures 2a–d and 3a–c) [52]. This spin-orbital splitting transition peak conformed from 50 to 88% of pure Ni^0 depending on the intensity of the spectra for each catalyst. However, low-intensity Ni $2p_{3/2}$ binding energy peaks originating at 853.2–855.5 eV were observed in all coatings corresponding to Ni^{2+} [53–55]. Moreover, the binding energy peak at 530.8 eV in the O1s spectra is assigned to $Ni(OH)_2$ (Figures 2 and 3) [53–55] and corresponds to up to ca. 25% of other compounds. Therefore, it can be claimed that all coatings have a small amount of nickel (II) hydroxide.

The Co $2p_{3/2}$ binding energy peak originating at 778.3 eV in Co2p spectra was also the most expressed for all Co-supported catalysts and corresponds to Co^0 (Figures 2e and 3d–f) [56]. The most expressed spin-orbital splitting transition peaks for Co2p conformed from 72 to 80% of pure Co^0 in Co-supported coatings. Co $2p_{3/2}$ binding energy peaks at 779.2 and 780.0 eV can be assigned to Co_3O_4 and CoO, respectively [53,56,57], and correspond to up to 24% of other compounds. The binding energy peaks at 529.8–531.7 eV in the O1s spectra are generally attributed to lattice oxygen species [58]. Therefore, the binding energy peak at 530.8 eV in the O1s spectra can also be associated with Co_3O_4 and CoO. The results show that Co-supported coatings also have a small amount of Co oxides. When analyzing the Mo3d XPS spectra, the most expressed binding energy peaks were obtained, originating at 228.0 eV and 231.2 eV for $Mo3d_{5/2}$ and $Mo3d_{3/2}$ transitions, respectively, corresponding to Mo^0 [59]. The most intensive spin-orbital splitting transition peaks for

Mn3d conformed from 32 to 38% of bare Mo^0 in Mo supported coatings. Two more binding energy peaks at 228.6 and 231.9 eV in the Mo 3d spectra correspond to Mo^{4+} [60]. Moreover, the binding energy peak at 530.8 eV in the O1s spectra is assigned to MoO_2 [59,60]. That means that in the Mo-supported coatings, a low amount of molybdenum oxide also exists. In all cases, the spin-orbital splitting transition peaks, with the binding energy peak at 530.8 eV, were attributed to the lattice oxygen species or hydroide depending on whether pure metal conformed up to 29% in all investigated coatings. It should be noted that for the O1s XPS spectra, higher binding energy peaks located at approximately 532–535 eV were usually attributed to the presence of the surface of adsorbed O_2, H_2O, and CO_2 (Figures 2 and 3) [58] and corresponding to up to ca. 65% of adsorbed compounds. Pure Ni, Co, and Mo metal phases predominate in all deposited coatings.

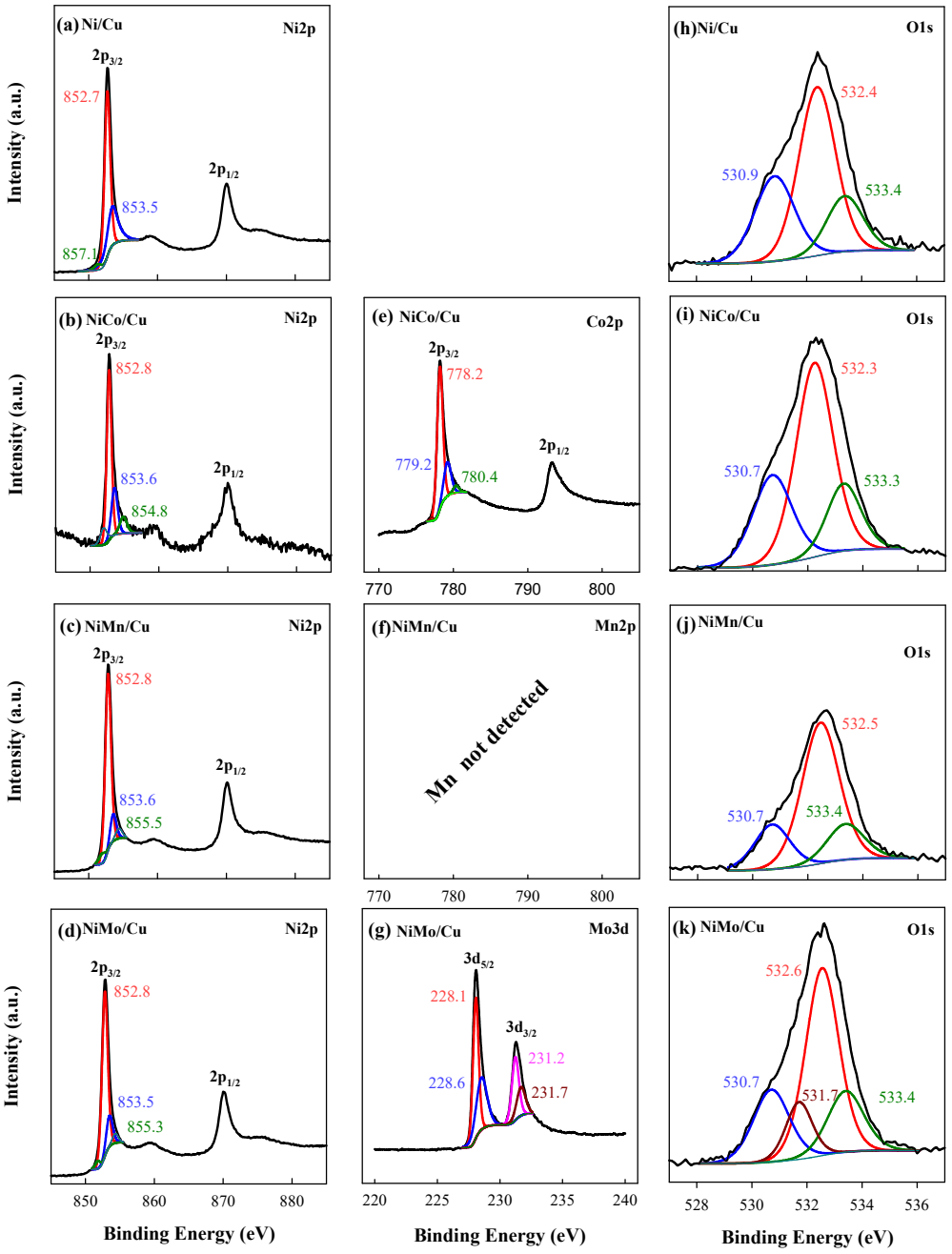

Figure 2. XPS spectra of Ni2p (**a**–**d**), Co2p (**e**), Mo 3d (**g**), and O1s (**h**–**k**) according to each catalyst. The amount of manganese in the NiMn/Cu (**f**) catalyst is too low to be identified.

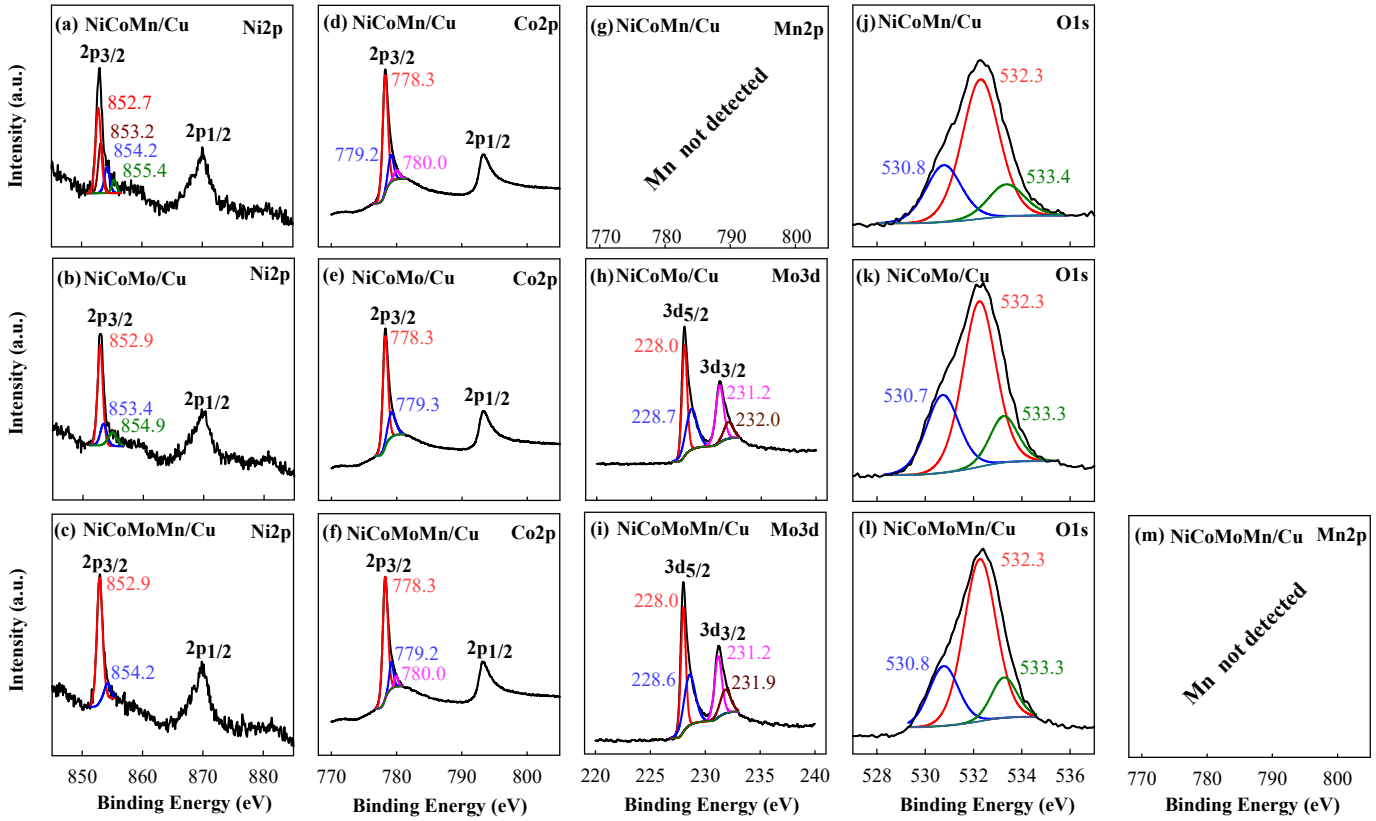

Figure 3. XPS spectra of Ni2p (**a**–**c**), Co2p (**d**–**f**), Mo 3d (**h**,**i**), and O 1s (**j**–**l**) according to each catalyst. The amount of manganese in the NiCoMn/Cu (**g**) and NiCoMoMn/Cu (**m**) catalysts is too low to be identified.

3.3. Catalytic Activity towards $NaBH_4$ Hydrolysis

Further, the catalytic activity of prepared catalysts towards $NaBH_4$ hydrolysis for hydrogen production was investigated in the solutions containing 5 wt% $NaBH_4$ + 0.4 wt% NaOH at the temperature range of 303–343 K.

The activation energy (E_a) of the hydrolysis reaction of $NaBH_4$ (Equation (1)) was calculated using the Arrhenius equation from the ln k versus 1/T graph (Equation (2)):

$$\ln k = \ln A - E_a/(RT) \quad (2)$$

where E_a is the activation energy (J), A is the pre-exponential factor, R is the general gas constant (8.314 J mol^{-1} K^{-1}), and k is the reaction rate coefficient.

Figures 4 and 5 present hydrogen generation rate graphs and Arrhenius plots for each catalyst. The summarized data are also given in Table 3. From the results obtained, it is seen that all prepared Ni/Cu, NiMn/Cu, NiMo/Cu, NiCo/Cu, NiCoMn/Cu, NiCoMo/Cu, and NiCoMoMn/Cu catalysts catalyze the hydrolysis of $NaBH_4$. Undoubtedly, HGR increases while increasing the temperature from 303 to 343 K. All multicomponent catalysts also exhibit greater HGR than pure Ni/Cu catalysts. Moreover, ternary- and four-component catalysts exhibit greater HGR than bi-component catalysts prepared for this work.

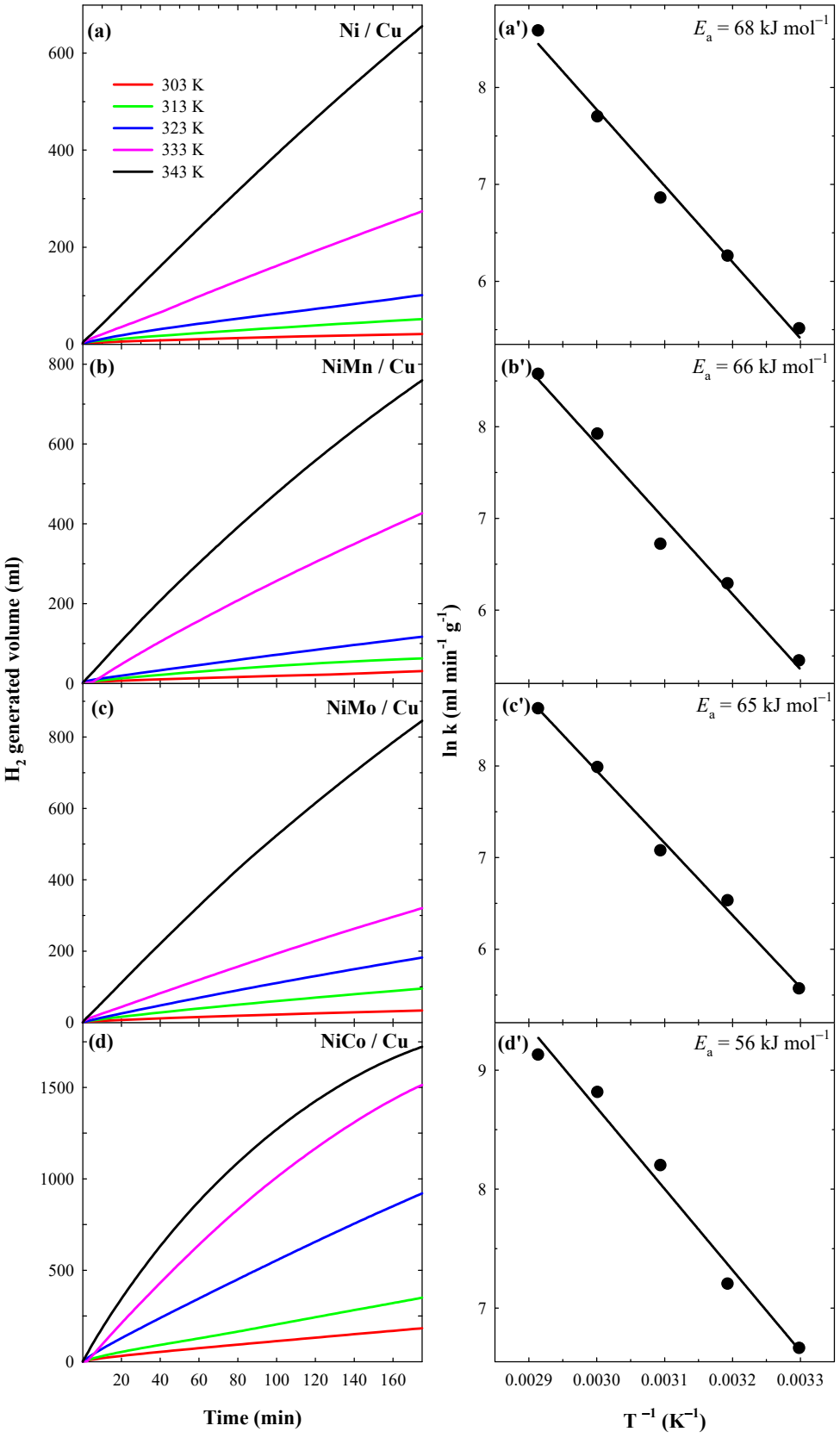

Figure 4. H_2 generation from 15 mL 5 wt% $NaBH_4$ + 0.4 wt% NaOH catalyzed by the Ni/Cu (**a**), NiMn/Cu (**b**), NiMo/Cu (**c**), and NiCo/Cu (**d**) catalysts at different temperatures; the corresponding Arrhenius plots (**a′**–**d′**). Dots show the amount of hydrogen released after 60 min at each temperature.

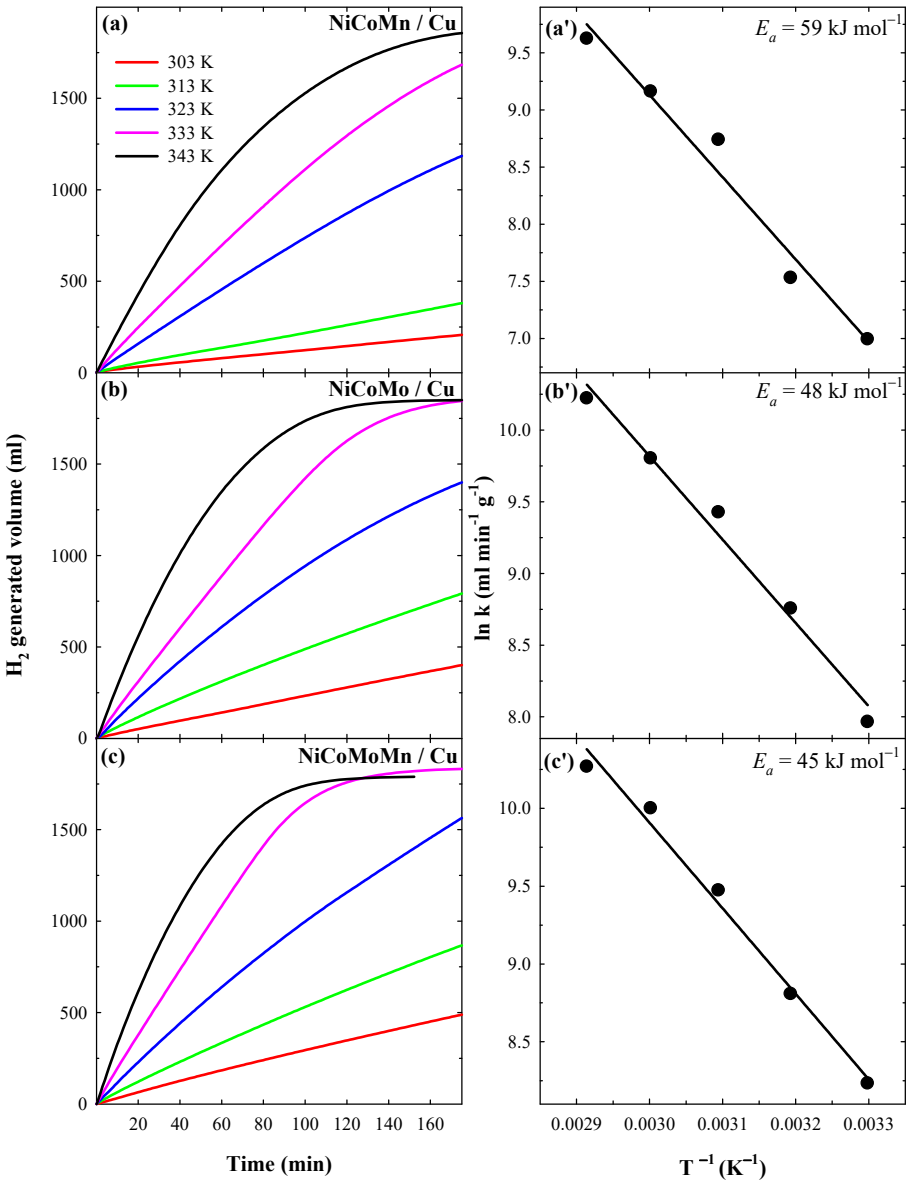

Figure 5. H_2 generation from 15 mL 5 wt% $NaBH_4$ + 0.4 wt% NaOH catalyzed by the NiCoMn/Cu (**a**), NiCoMo/Cu (**b**), and NiCoMoMn/Cu (**c**) catalysts at different temperatures; the corresponding Arrhenius plots (**a′**–**c′**). Dots show the amount of hydrogen released after 60 min at each temperature.

Let us discuss each group in detail. At first, when the temperature increases from 303 to 343 K, the HGR for the pure Ni/Cu catalyst rises from 0.18 to 3.99 mL min^{-1}. When using bi-component NiCo/Cu, NiMn/Cu, and NiMo/Cu catalysts for hydrogen generation by hydrolysis of $NaBH_4$ with an increasing temperature, HGR increases from 1.24 to 14.59 mL min^{-1} for the NiCo/Cu catalyst, from 0.22 to 5.03 mL min^{-1} for the NiMn/Cu catalyst, and from 0.26 to 5.45 mL min^{-1} for the NiMo/Cu catalyst, respectively (Figure 4a–d, Table 3), and it is higher compared to Ni/Cu. The data show that HGR is 22% and 44% higher using NiMn/Cu and NiMo/Cu, respectively, than the Ni/Cu catalysts at 30 °C temperature (Table 3). Comparing these two catalysts, NiMo/Cu activity for the hydrogen generation reaction is higher by 18% than NiMn/Cu. As was mentioned above, it is difficult to deposit a larger amount of Mn^0; however, even a significantly small quantity of Mn in the coating (0.16 wt%) increases the efficiency of the NiMn/Cu catalyst compared with the Ni/Cu catalyst (Table 3). As is evident, NiCo/Cu demonstrated the highest activity for $NaBH_4$ hydrolysis from these three investigated bi-component catalysts. The

H_2 generation rate was 5–7 times higher on the NiCo/Cu catalysts than on the NiMn/Cu or NiMo/Cu catalysts in the 5 wt% $NaBH_4$ + 0.4 wt% NaOH solution at 303 K. At the highest experimental temperature (343 K), the activity of bi-component catalysts remained the same. All three bi-component catalysts outperformed the activity of pure Ni/Cu for $NaBH_4$ hydrolysis. The HGR was 26% and 37% higher on NiMn/Cu and NiMo/Cu, respectively, than on the Ni/Cu catalyst at 343 K. It was observed that the activity of NiMo/Cu slightly decreased (44% at 303 K and 37% at 343 K). This may occur due to spontaneous hydrolysis of the borohydride at high temperatures. So, comparing the NiMn/Cu and NiMo/Cu catalysts, the NiMo/Cu exhibited 7.7% higher activity for hydrogen generation. However, here, the same trend remains, and the NiCo/Cu catalyst shows 3–4 times higher activity for $NaBH_4$ hydrolysis compared with NiMn/Cu, NiMo/Cu, Ni/Cu in a reaction bath at 343 K (Table 3).

Table 3. H_2 generation rates and activation energies for the prepared catalysts.

Catalysts	E_a, kJ mol^{-1}	T, K	v, mL min^{-1}
Ni/Cu	67.9	303 K	0.18
		313 K	0.39
		323 K	0.77
		333 K	1.64
		343 K	3.99
NiCo/Cu	56.4	303 K	1.24
		313 K	2.13
		323 K	5.77
		333 K	10.66
		343 K	14.59
NiMn/Cu	66.1	303 K	0.22
		313 K	0.66
		323 K	1.38
		333 K	2.53
		343 K	5.03
NiMo/Cu	65.5	303 K	0.26
		313 K	0.49
		323 K	1.16
		333 K	2.00
		343 K	5.45
NiCoMn/Cu	58.8	303 K	1.33
		313 K	2.30
		323 K	5.05
		333 K	11.6
		343 K	18.41
NiCoMo/Cu	48.3	303 K	2.35
		313 K	2.84
		323 K	6.51
		333 K	14.80
		343 K	22.47
NiCoMoMn/Cu	45.3	303 K	3.08
		313 K	5.47
		323 K	8.79
		333 K	18.03
		343 K	23.57

According to the Arrhenius plots (Figure 4a′–d′), the activation energy for the $NaBH_4$ hydrolysis catalyzed by bi-component NiCo/Cu, NiMn/Cu, NiMo/Cu coatings was calculated to be 56.4, 66.1 and 65.5 kJ mol^{-1}, respectively, and was lower than on pure

Ni/Cu (67.9 kJ mol^{-1}). As is evident from the bi-component catalysts, the lowest activation energy for the $NaBH_4$ hydrolysis was obtained for the NiCo/Cu catalyst (Figure 4d′).

It can be clearly seen that the incorporation of Co into the Ni/Cu coating significantly improves the catalytic activity of the newly prepared NiCo/Cu catalyst for the $NaBH_4$ hydrolysis reaction. Therefore, it was decided to deposit ternary-component coatings by incorporating Co into NiMn and NiMo coatings.

The catalytic activity results of the prepared ternary-component NiCoMn/Cu and the NiCoMo/Cu catalysts towards $NaBH_4$ hydrolysis for hydrogen production in 5 wt% $NaBH_4$ + 0.4 wt% NaOH solution is shown in Figure 5 and Table 3. As can be seen from the results, the incorporation of cobalt in NiMn and NiMo significantly decreases the activation energies of prepared ternary-component NiCoMn/Cu (58.8 kJ mol^{-1}) and the NiCoMo/Cu (48.3 kJ mol^{-1}) catalysts compared with bi-component ones (Figure 5a′,b′, Table 3). Ternary-component catalysts also showed higher HGR at 303–343 K (Figure 5a,b, Table 3). At the lowest temperature (303 K) of the working bath, after inserting Co, the release of hydrogen accelerates 83% for the NiCoMn/Cu catalyst and 89% for the NiCoMo/Cu catalyst. At the highest temperature (343 K) of the working bath, the incorporation of Co increases the release of hydrogen by approximately 75% for both ternary-component catalysts compared with bi-component NiMn/Cu and NiMo/Cu catalysts.

Finally, all four Ni, Co, Mn, and Mo metals were combined to obtain a four-component NiCoMoMn/Cu catalyst. It was a noteworthy decision because the co-precipitation of all of the metals in one coating led to the creation of this study's most effective catalyst for $NaBH_4$ hydrolysis.

According to the Arrhenius plots (Figure 5c′), the activation energy for the $NaBH_4$ hydrolysis catalyzed by the NiCoMoMn/Cu catalyst was calculated to be 45.3 kJ mol^{-1} and was the lowest one among all of the investigated catalysts. Undoubtedly, the volume of hydrogen evolved (3.08–23.57 mL min^{-1}) in the 303–343 K temperature range was also the highest on this catalyst (Figure 5c, Table 3). The NiCoMoMn/Cu catalyst exhibited 24% and 57% higher catalytic efficiency for hydrogen generation than NiCoMo/Cu and NiCoMn/Cu, respectively, at the lowest temperature (303 K) of the working bath. The NiCoMoMn/Cu catalyst also showed 5% and 22% enhanced catalytic activity for the hydrogen generation at the highest temperature (303 K) of the working bath, respectively, than on NiCoMo/Cu and NiCoMn/Cu. This might be due to the high specific surface of the cauliflower-like nanostructure and the synergistic effect of metals in catalysts [26].

While the NiCoMoMn/Cu catalyst was established as the most efficient catalyst for the $NaBH_4$ hydrolysis among the other catalysts presented in this work, the stability test was carried out by reusing NiCoMoMn/Cu in five cycles of the hydrogen generation in the 5 wt% $NaBH_4$ and 5 wt% NaOH solution at 323 K. At the end of each cycle, the catalyst was washed several times with deionized water, dried, and used repeatedly. Figure 6 shows that the hydrogen production rate slightly declined from 1164 to 1124 mL min^{-1}. However, noticeable differences were not observed. It was calculated that the NiCoMoMn/Cu catalyst retained 96.5% of its initial catalytic activity for the $NaBH_4$ hydrolysis after the completion of the fifth cycle, and it is higher compared with some others described in the literature [61,62].

The obtained data suggest that combining and incorporating additional metals into the coatings creates a stronger synergistic effect between metals, making the catalysts more efficient for the hydrogen generation reaction.

The activation energies (E_a) of the proposed NiMn/Cu, NiMo/Cu, NiCo/Cu, NiCoMn/Cu, NiCoMo/Cu, and NiCoMoMn/Cu catalysts were compared with others reported in the literature (Table 4). It is seen that our prepared four-component NiCoMoMn/Cu catalyst exhibited the lowest activation energy, 45.30 kJ mol^{-1}, if compared with other catalysts presented in Table 4. As well as our prepared ternary-component NiCoMo/Cu catalyst having an activation energy of 48.30 kJ mol^{-1}, it also outperformed the similar NiCoMo [49] catalyst reported in the literature. As is evident from the data given in Table 4, our prepared catalysts exhibited lower activation energies than those previously reported.

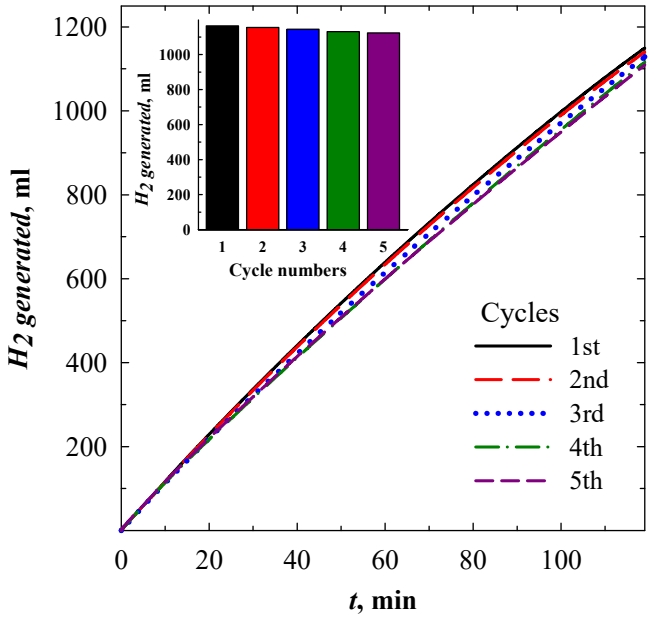

Figure 6. Reusability of NiCoMoMn/Cu catalyst after five cycles in 5 wt% $NaBH_4$ + 0.4 wt% NaOH solution.

Table 4. The comparison of the activation energies (E_a).

Catalysts	$NaBH_4$ Solution	E_a, kJ mol^{-1}	References
Ni	5 wt% $NaBH_4$ + 0.1 M NaOH	67.90	in this work
Ni	5 wt% $NaBH_4$ + 10 wt% NaOH	72.52	[30]
NiCo	5 wt% $NaBH_4$ + 0.1 M NaOH	56.40	in this work
NiCo	2.7 wt% $NaBH_4$ + 15 wt% NaOH	62.00	[31]
NiCoP	0.3 M $NaBH_4$ + 10 wt% NaOH	57.00	[63]
CoMo	5 wt% $NaBH_4$ + 7 wt% NaOH	51.00	[26]
Co	10 wt% $NaBH_4$ + 1 wt% NaOH	60.20	[64]
Co	20 wt% $NaBH_4$ + 5 wt% NaOH	64.90	[65]
NiMn	5 wt% $NaBH_4$ + 0.1 M NaOH	66.10	in this work
NiMo	5 wt% $NaBH_4$ + 0.1 M NaOH	65.50	in this work
NiCoMn	5 wt% $NaBH_4$ + 0.1 M NaOH	58.80	in this work
NiCoMo	5 wt% $NaBH_4$ + 0.1 M NaOH	48.30	in this work
NiCoMo	7 wt% $NaBH_4$ + 10 wt% NaOH	52.43	[49]
NiCoMoMn	5 wt% $NaBH_4$ + 0.1 M NaOH	45.30	in this work

4. Conclusions

Herein, a simple electroless deposition method for Ni, Co, Mn, and Mo plating on Cu surfaces was described. The bi-component NiMn/Cu, NiMo/Cu, NiCo/Cu, ternary-component NiCoMn/Cu, NiCoMo/Cu, and four-component NiCoMoMn/Cu catalysts were prepared, and their activity for sodium borohydride hydrolysis reaction was investigated.

It was found that the Ni/Cu, NiMn/Cu, NiMo/Cu, NiCo/Cu, NiCoMn/Cu, NiCoMo/Cu, and NiCoMoMn/Cu catalysts demonstrated increased catalytic activity for sodium borohydride hydrolysis reaction with increased metal components in the coating. The activation energy decreased in the line Ni/Cu > NiMn/Cu > NiMo/Cu > NiCoMn/Cu > NiCo/Cu > NiCoMo/Cu > NiCoMoMn/Cu, and was equal to 67.9 > 66.1 > 65.5 > 58.8 > 56.4 > 48.3 > 45.3 kJ mol^{-1}, respectively.

As it is seen, the lowest activation energy of 45.3 kJ mol^{-1} for sodium borohydride hydrolysis reaction was obtained using a four-component NiCoMoMn/Cu catalyst. The highest hydrogen generation rate was achieved using this four-component catalyst. By increasing the temperature from 303 K to 343 K, the generated amount of H_2 increased 7.7 times from 3.08 mL min^{-1} to 23.57 mL min^{-1}. The higher efficiency of multicomponent catalysts for hydrogen generation from the $NaBH_4$ hydrolysis reaction may be related to the synergistic effect between the metals in a coating and also to surface morphology. In addition, the presence of Mn possibly results in the formation of nanosphere structures

with larger exposed surfaces, leading to an improvement in the catalytic performance of the catalyst.

The data obtained suggest proposing the simply prepared NiCoMoMn/Cu catalyst for the efficient hydrogen generation from alkaline sodium borohydride solution by hydrolysis.

Author Contributions: Conceptualization, Z.S. and V.K.; methodology, V.J., G.S. and J.V.; formal analysis, G.V.; investigation, G.V. and I.S.; data curation, Z.S.; writing—original draft preparation, V.K. and Z.S.; writing—review and editing, E.N. and L.T.-T.; visualization, E.N., Z.S. and L.T.-T.; and supervision, Z.S. and L.T.-T. All authors have read and agreed to the published version of the manuscript.

Funding: This research received no external funding.

Institutional Review Board Statement: Not applicable.

Informed Consent Statement: Not applicable.

Data Availability Statement: Not applicable.

Conflicts of Interest: The authors declare no conflict of interest.

References

1. Tarhan, C.; Cil, M.A. A study on hydrogen, the clean energy of the future: Hydrogen storage methods. *J. Energy Storage* **2021**, *40*, 102676. [CrossRef]
2. Younas, M.; Shafique, S.; Hafeez, A.; Javed, F.; Rehman, F. An overview of hydrogen production: Current status, potential, and challenges. *Fuel* **2022**, *316*, 123317. [CrossRef]
3. Van Hoecke, L.; Laffineur, L.; Campe, R.; Perreault, P.; Verbruggen, S.W.; Lenaerts, S. Challenges in the use of hydrogen for maritime applications. *Energy Environ. Sci.* **2021**, *14*, 815. [CrossRef]
4. Chen, Z.; Kirlikovali, K.O.; Idrees, K.B.; Wasson, M.C.; Farha, O.K. Porous materials for hydrogen storage. *Chemisty* **2022**, *8*, 693. [CrossRef]
5. Yao, Q.; Ding, Y.; Lu, Z.H. Noble-metal-free nanocatalysts for hydrogen generation from boron- and nitrogen-based hydrides. *Inorg. Chem. Front.* **2020**, *7*, 3837. [CrossRef]
6. Ekinci, A. Hydrogen generation by hydrolysis of $NaBH_4$ with efficient Co–La–Mo–B catalyst for PEM fuel cells. *Kinet. Catal.* **2020**, *61*, 589. [CrossRef]
7. Bozkurt, G.; Ozer, A.; Yurtcan, A.B. Development of effective catalysts for hydrogen generation from sodium borohydride: Ru, Pt, Pd nanoparticles supported on Co_3O_4. *Energy* **2019**, *180*, 702. [CrossRef]
8. IEA. *Global Hydrogen Review*; License: CC BY 4.0; IEA: Paris, France, 2022; Available online: https://www.iea.org/reports/global-hydrogen-review-2022 (accessed on 15 August 2023).
9. Hydrogen to the rescue. *Nat. Mater.* **2018**, *17*, 565. [CrossRef]
10. *Hydrogen Insights: A Perspective on Hydrogen Investment, Market Development and Cost Competitiveness*; Hydrogen Council and McKinsey & Company: Brussels, Belgium, 2021.
11. Altaf, C.T.; Colak, T.O.; Minkina, V.G.; Shabunya, S.I.; Sankir, M.; Sankir, N.D.; Kalinin, V.I. Effect of titanium dioxide support for cobalt nanoparticle catalysts for hydrogen generation from sodium borohydride hydrolysis. *Catal. Lett.* **2022**, 287. [CrossRef]
12. Yang, F.; Ruan, J.; Li, T.; Zou, Y.; Xiang, C.; Xu, F.; Sun, L. Hydrolysis of sodium borohydride using a highly stable catalyst of ruthenium nanoparticles supported by cobalt–nickel hydroxide-coated nickel foam. *J. Alloys Compd.* **2022**, *926*, 166902. [CrossRef]
13. Ouyang, L.; Liu, M.; Chen, K.; Liu, J.; Wang, H.; Zhu, M.; Yartys, V. Recent progress on hydrogen generation from the hydrolysis of light metals and hydrides. *J. Alloys Compd.* **2022**, *910*, 164831. [CrossRef]
14. Comanescu, C. Paving the way to the fuel of the future—Nanostructured complex hydrides. *Int. J. Mol. Sci.* **2023**, *24*, 143. [CrossRef]
15. Dragan, M. Hydrogen storage in complex metal hydrides $NaBH_4$: Hydrolysis reaction and experimental strategies. *Catalysts* **2022**, *12*, 356. [CrossRef]
16. Abdelhamid, H.N. A review on hydrogen generation from the hydrolysis of sodium borohydride. *Int. J. Hydrogen Energy* **2021**, *46*, 726. [CrossRef]
17. Hansu, T.A.; Sahin, O.; Caglar, A.; Kivrak, H. A remarkable Mo doped Ru catalyst for hydrogen generation from sodium borohydride: The effect of Mo addition and estimation of kinetic parameters. *React. Kinet. Mech. Catal.* **2020**, *131*, 661. [CrossRef]
18. Yu, Y.; Kang, L.; Sun, L.; Xu, F.; Pan, H.; Sang, Z.; Zhang, C.; Jis, X.; Sui, Q.; Bu, Y.; et al. Bimetallic Pt-Ni nanoparticles confined in porous titanium oxide cage for hydrogen generation from $NaBH_4$ hydrolysis. *Nanomaterials* **2022**, *12*, 2550. [CrossRef]
19. Hashimi, A.S.; Nohan, M.A.N.M.; Chin, S.X.; Khiew, P.S.; Zakaria, S.; Chia, C.H. Copper nanowires as highly efficient and recyclable catalyst for rapid hydrogen generation from hydrolysis of sodium borohydride. *Nanomaterials* **2020**, *10*, 1153. [CrossRef]

20. Ruslan, N.; Yahya, M.S.; Siddique, M.N.I.; Yengantiwar, A.P.; Ismail, M.; Awal, M.R.; Yusoff, M.Z.M.; Yap, M.F.A.A.H.; Mustafa, N.S. Review on magnesium hydride and sodium borohydride hydrolysis for hydrogen production. *Crystals* **2022**, *12*, 1376. [CrossRef]
21. Markovic, N.; Gasteiger, H.; Ross, P.N. Kinetics of oxygen reduction on Pt(hkl) electrodes: Implications for the crystallite size effect with supported Pt electrocatalysts. *J. Electrochem. Soc.* **1997**, *144*, 1591. [CrossRef]
22. Liang, Y.; Dai, H.B.; Ma, L.P.; Wang, P.; Cheng, H.M. Hydrogen generation from sodium borohydride solution using a ruthenium supported on graphite catalyst. *Int. J. Hydrogen Energy* **2010**, *35*, 3023. [CrossRef]
23. Hsieh, C.T.; Huang, C.L.; Chen, Y.A.; Lu, S.Y. NiFeMo alloy inverse-opals on Ni foam as outstanding bifunctional catalysts for electrolytic water splitting of ultra-low cell voltages at high current densities. *Appl. Catal. B Environ.* **2020**, *267*, 118376. [CrossRef]
24. Wei, Y.; Meng, W.; Wang, Y.; Gao, Y.; Qi, K.; Zhang, K. Fast hydrogen generation from $NaBH_4$ hydrolysis catalyzed by nanostructured Co-Ni-B catalysts. *Int. J. Hydrogen Energy* **2017**, *42*, 6072. [CrossRef]
25. Wang, Y.; Li, G.; Wu, S.; Wei, Y.; Meng, W.; Xie, Y.; Cui, Y.; Lian, X.; Chen, Y.; Zhang, X. Hydrogen generation from alkaline $NaBH_4$ solution using nanostructured Co-Ni-P catalysts. *Int. J. Hydrogen Energy* **2017**, *42*, 16529. [CrossRef]
26. Wei, Y.; Wang, R.; Meng, L.; Wang, Y.; Li, G.; Xin, S.; Zhao, X.; Zhang, K. Hydrogen generation from alkaline $NaBH_4$ solution using a dandelion-like Co-Mo-B catalyst supported on carbon cloth. *Int. J. Hydrogen Energy* **2017**, *42*, 9945. [CrossRef]
27. Akkus, M.S. Examination of the catalytic effect of Ni, NiCr, and NiV catalysts prepared as thin films by magnetron sputtering process in the hydrolysis of sodium borohydride. *Int. J. Hydrogen Energy* **2023**, *48*, 23055. [CrossRef]
28. Keskin, M.S.; Ağırtaş, M.S. Hydrogen production performance and kinetic behavior from sodium borohydride hydrolysis with TiO2-supported Co-Mo-B catalyst. *Ionics* **2023**, *29*, 3713. [CrossRef]
29. Wei, Y.; Wang, M.; Fu, W.; Si, S.; Wei, L.; Zhao, X.; Wang, Y. Mn doped CoP/Ni foam catalyst for hydrogen generation from hydrolysis of sodium borohydride. *Mater. Lett.* **2022**, *308*, 131166. [CrossRef]
30. Liang, Z.; Li, Q.; Li, F.; Zhao, S.; Xia, X. Hydrogen generation from hydrolysis of $NaBH_4$ based on high stable $NiB/NiFe_2O_4$ catalyst. *Int. J. Hydrogen Energy* **2017**, *42*, 3971. [CrossRef]
31. Ingersoll, J.C.; Mani, N.; Thenmozhiyal, J.C.; Muthaiah, A. Catalytic hydrolysis of sodium borohydride by a novel nickel–cobalt–boride catalyst. *J. Power Sources* **2007**, *173*, 450. [CrossRef]
32. Zhang, P.; Lv, Z.; Liu, X.; Xie, G.; Zhang, B. Electroless nickel plating on alumina ceramic activated by metallic nickel as electrocatalyst for oxygen evolution reaction. *Catal. Commun.* **2021**, *149*, 106238. [CrossRef]
33. Sabeen, A.H.; Kamaruddin, S.N.B.; Noor, Z.Z. Environmental impacts assessment of industrial wastewater treatment system using electroless nickel plating and life cycle assessment approaches. *Int. J. Environ. Sci. Technol.* **2019**, *16*, 3171. [CrossRef]
34. Baboria, M.; Pathania, A.S. An analytical investigation pertaining to autocatalytic plating of chromium nickel carbide powder on copper alloys using electroless deposition method. *World J. Adv. Res. Rev.* **2023**, *17*, 291. [CrossRef]
35. Takeoka, H.; Seike, M.; Nakamura, Y.; Imai, H.; Oaki, Y.; Fujii, S. Electroless nickel plating on a biomineral-based sponge structure. *Mater. Adv.* **2022**, *3*, 931. [CrossRef]
36. Thakur, A.; Gharde, S.; Kandasubramanian, B. Electroless nickel fabrication on surface modified magnesium substrates. *Def. Technol.* **2019**, *15*, 636. [CrossRef]
37. Huang, Z.; Nguyen, T.T.; Zhou, Y.; Qi, G. A low temperature electroless nickel plating chemistry. *Surf. Coat. Technol.* **2019**, *372*, 160. [CrossRef]
38. Izgia, M.S.; Onata, E.; Kazicib, H.C.; Sahin, O. Hydrogen production through the cooperation of a catalystsynthesized in ethanol medium and the effect of the plasma. *Energy Sources Part A Recovery Util. Environ. Eff.* **2019**, *45*, 8271. [CrossRef]
39. Sukackienė, Z.; Jasulaitienė, V.; Naujokaitis, A.; Tamašauskaitė-Tamašiūnaitė, L.; Norkus, E. Electroless deposition of CoBW coatings using morpholine borane as a reducing agent. *Thin Solid Film.* **2017**, *636*, 425. [CrossRef]
40. Kumar, M.; Bhavani, T.; Rawal, S.; Sidpara, A. Magnetorheological finishing of chemically treated electroless nickel plating. *Magnetochemistry* **2022**, *8*, 184. [CrossRef]
41. Li, Y.; Deng, X.; Lei, M.; Li, X.; Ouyang, H. Enhancing the properties of the SAC305-soldered joint: Heat treatment of the nickel-plated copper substrate before reflow soldering. *J. Mater. Sci. Mater. Electron.* **2022**, *33*, 3535. [CrossRef]
42. Gomes, N.; Gonzalez-Estrada, O.A.; Pertuz, A. Electroless nickel phosphorous: A global vision. *Rev. UIS Ing.* **2019**, *18*, 173. [CrossRef]
43. Zhao, F.; Hu, H.; Yu, J.; Lai, J.; He, H.; Zhang, Y.; Qi, H.; Wang, D. Mechanical and tribological properties of Ni-B and Ni-B-W coatings prepared by electroless plating. *Lubricants* **2023**, *11*, 42. [CrossRef]
44. Tsai, M.H.; Chen, T.C.; Juang, Y.; Hua, L.C.; Huang, C. High catalytic performance of CuCo/nickel foam electrode for ammonia electrooxidation. *Electrochem. Commun.* **2020**, *121*, 106875. [CrossRef]
45. Wang, L.; Liu, D.; Zhang, Z.; Li, Y.; Liu, J.; Yang, Y.; Xue, B.; Li, F. Self-adaptively electrochemical reconstruction of NiFe-layered double hydroxide on Ni foam for high-performance water splitting. *J. Alloys Compd.* **2023**, *934*, 167846. [CrossRef]
46. Kytsya, A.; Berezovets, V.; Verbovytskyy, Y.; Bazylyak, L.; Kordan, V.; Zavaliy, I.; Yartys, V.A. Bimetallic Ni-Co nanoparticles as an efficient catalyst of hydrogen generation via hydrolysis of $NaBH_4$. *J. Alloys Compd.* **2022**, *908*, 164484. [CrossRef]
47. Hu, X.; Tian, X.; Lin, Y.W.; Wang, Z. Nickel foam and stainless steel mesh as electrocatalysts for hydrogen evolution reaction, oxygen evolution reaction and overall water splitting in alkaline media. *R. Soc. Chem.* **2019**, *9*, 31563. [CrossRef]
48. Jiang, X.; Xu, W.; Lai, S.; Chen, X. Integral structured Co–Mn composite oxides grown on interconnected Ni foam for catalytic toluene oxidation. *R. Soc. Chem.* **2019**, *9*, 6533. [CrossRef]

49. Wang, L.; Li, Z.; Zhang, P.; Wang, G.; Xie, G. Hydrogen generation from alkaline $NaBH_4$ solution using CoNiMoP/g-Al_2O_3 catalysts. *Int. J. Hydrogen Energy* **2016**, *41*, 1468. [CrossRef]
50. Sukackienė, Z.; Antanavičiūtė, K.; Vaičiūnienė, J.; Tamašauskaitė-Tamašiūnaitė, L.; Naujokaitis, A.; Norkus, E. Electroless deposition of nickel-boron coatings. *Chemija* **2020**, *31*, 1. [CrossRef]
51. Tarozaitė, R.; Sudavičius, A.; Sukackienė, Z.; Norkus, E. Electroless cobalt deposition in the glycinate soliution using morpholine borane as a reducing agen. *Trans. Inst. Mater. Finish.* **2014**, *92*, 146. [CrossRef]
52. X-ray Photoelectron Spectroscopy (XPS) Reference Pages. Available online: http://www.xpsfitting.com/search/label/Nickel (accessed on 16 August 2023).
53. Biesinger, M.C.; Payne, B.P.; Lau, L.W.M.; Gerson, A.R.; Smart, R.S.C. X-ray photoelectron spectroscopic chemical state quantification of mixed nickel metal, oxide and hydroxide systems. *Surf. Interface Anal.* **2009**, *41*, 324. [CrossRef]
54. Biesinger, M.C.; Payne, B.P.; Grosvenor, A.P.; Lau, L.W.M.; Gerson, A.R.; Smart, R.S.C. Resolving surface chemical states in XPS analysis of first row transition metals, oxides and hydroxides: Cr, Mn, Fe, Co and Ni. *Appl. Surf. Sci.* **2011**, *257*, 2717. [CrossRef]
55. X-ray Photoelectron Spectroscopy (XPS) Reference Pages. Available online: http://www.xpsfitting.com/search/label/Oxygen (accessed on 17 August 2023).
56. X-ray Photoelectron Spectroscopy (XPS) Reference Pages. Available online: http://www.xpsfitting.com/search/label/Cobalt (accessed on 16 August 2023).
57. Yang, J.; Liu, H.; Martens, W.N.; Frost, R.L. Synthesis and characterization of cobalt hydroxide, cobalt oxyhydroxide, and cobalt oxide nanodiscs. *J. Phys. Chem. C* **2010**, *114*, 111. [CrossRef]
58. Hsieh, P.-T.; Chen, Y.-C.; Kao, K.S.; Wang, C.M. Luminescence mechanism of ZnO thin film investigated by XPS measurement. *Appl. Phys. A* **2008**, *90*, 317. [CrossRef]
59. X-ray Photoelectron Spectroscopy (XPS) Reference Pages. Available online: http://www.xpsfitting.com/search/label/Molybdenum (accessed on 16 August 2023).
60. NIST X-ray Photoelectron Spectroscopy Database. Available online: http://srdata.nist.gov/xps/ (accessed on 16 August 2023).
61. Sanchez, F.; Motta, D.; Roldan, A.; Hammond, C.; Villa, A.; Dimitratos, N. Hydrogen Generation from Additive-Free Formic Acid Decomposition Under Mild Conditions by Pd/C: Experimental and DFT Studies. *Top. Catal.* **2018**, *61*, 254. [CrossRef]
62. Soltani, M.; Zabihi, M. Hydrogen generation by catalytic hydrolysis of sodium borohydride using the nano-bimetallic catalysts supported on the core-shell magnetic nanocomposite of activated carbon. *Int. J. Hydrogen Energy* **2020**, *45*, 12331. [CrossRef]
63. Rakapa, M.; Kalua, E.E.; Özkar, S. Cobalt–nickel–phosphorus supported on Pd-activated TiO_2 (Co–Ni–P/Pd-TiO_2) as cost-effective and reusable catalyst for hydrogen generation from hydrolysis of alkaline sodium borohydride solution. *J. Alloys Compd.* **2011**, *509*, 7016. [CrossRef]
64. Eom, K.; Cho, K.; Kwon, H. Effects of electroless deposition conditions on microstructures of cobalt–phosphorous catalysts and their hydrogen generation properties in alkaline sodium borohydride solution. *J. Power Sources* **2008**, *180*, 484. [CrossRef]
65. Jeong, S.U.; Kima, R.K.; Cho, E.A.; Kimb, H.J.; Namb, S.W.; Oh, I.H.; Hong, S.A.; Kim, S.H. A study on hydrogen generation from $NaBH_4$ solution using the high-performance Co-B catalyst. *J. Power Sources* **2005**, *144*, 129. [CrossRef]

Disclaimer/Publisher's Note: The statements, opinions and data contained in all publications are solely those of the individual author(s) and contributor(s) and not of MDPI and/or the editor(s). MDPI and/or the editor(s) disclaim responsibility for any injury to people or property resulting from any ideas, methods, instructions or products referred to in the content.